iScience

CellPress
OPEN ACCESS

Article

# Exploring heparin's protective mechanism against AGEs induced endothelial injury

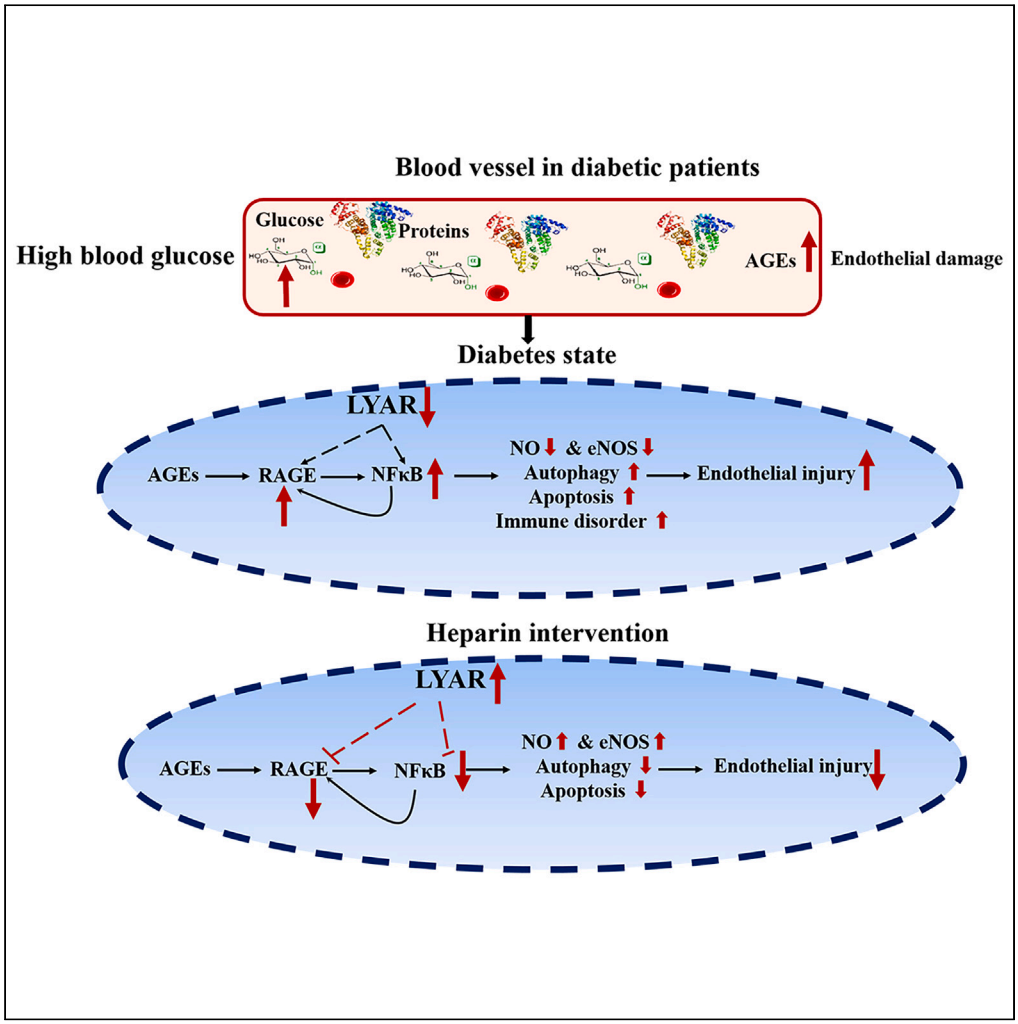


Junfeng Shi, Yudong Guan, Hongwei Song, ..., Ming Shan, Xiaodong Sun, Hongyan Qiu

xiaodong.sun@sdsmu.edu.cn (X.S.)
qiuhongyan@sdsmu.edu.cn (H.Q.)

## Highlights

Heparin has the potential to ameliorate AGEs-induced endothelial injury

Heparin inhibited AGEs-RAGE-NFκB axis, mitigating endothelial inflammatory

Heparin exert positive influence by upregulating LYAR

Shi et al., iScience 27, 111084
November 15, 2024 
https://doi.org/10.1016/j.isci.2024.111084

iScience

CellPress
OPEN ACCESS

Article

# Exploring heparin's protective mechanism against AGEs induced endothelial injury

Junfeng Shi,[1,2,8] Yudong Guan,[3,8] Hongwei Song,[1,2,8] Liang Zhu,[1,2] Jingjing Li,[4] Qinying Li,[1,2] Ningning Hou,[1] Fang Han,[1,2,5] Meng Wang,[6] Kexin Zhang,[1,2] Ming Shan,[7] Xiaodong Sun,[1,2,*] and Hongyan Qiu[1,2,9,*]

## SUMMARY

**Advanced glycation end products (AGEs) in diabetes can cause endothelial damage. Heparin, widely known as a recognized anticoagulant, is also a multifunctional therapeutic drug. This study investigated whether heparin could ameliorate AGEs-induced endothelial injury. Remarkably, heparin effectively attenuated this cellular damage and assumed a reparative role. Furthermore, heparin inhibited the AGEs-RAGE-NFκB axis, thereby mitigating endothelial inflammatory injury. Comprehensive proteome and knockdown experiments suggested that heparin may exert a positive influence on cell growth and further alleviate pathological damage by upregulating the expression of LYAR (cell growth-regulating nucleolar protein). Diabetic mouse model was also used to further verify the changes of endothelial tissue in diabetic state and heparin intervention. In summary, these findings demonstrate that heparin has the potential to ameliorate AGEs-induced endothelial injury, opening new avenues for exploring the expanded therapeutic roles of heparin and its potential application in the management of diabetes and its associated complications.**

## INTRODUCTION

Diabetes mellitus (DM) is characterized by chronic metabolic disorders and persistently elevated blood glucose levels.[1] This condition is accompanied by various complications, among which kidney disease and cardiovascular disease are the most common, leading to an unfavorable prognosis in the majority of patients.[2–5] Thus, there is an urgent need to develop effective prevention and treatment strategies for diabetes and its associated complications.

The persistent accumulation of glucose in both microvascular and macrovascular environments initiates a series of reactions, involving the carbonyl groups of glucose that react with amino groups of proteins. These reactions culminate in the irreversible formation of advanced glycation end products (AGEs).[6–9] AGEs play a pivotal role in various pathological changes, primarily through their activation of the receptor for advanced glycation end products (RAGE) located on cell membranes. The AGEs-RAGE signaling pathway mediates the expression of many molecules, such as NF-κB, MAPK (mitogen-activated protein kinase)/ERK (extracellular signal-regulated kinase), and PI3K(phosphatidylinositol 3-kinase) /Akt (protein kinase B), which in turn accelerate the progression of inflammation.[10] Subsequently, this cascade of events leads to decreased endothelial nitric oxide synthase (eNOS)/nitric oxide (NO) levels, increased adhesion molecule and chemokine expression, and the disruption of vascular function and blood pressure homeostasis.[10,11] The loss of homeostasis in blood vessels and tissues precipitates immune dysfunction and apoptosis *in vivo*.[12,13] RAGE activation in endothelial cells leads to cellular structural disorders and dysfunction, contributing to the increasing incidence of complications.[14,15] Notably, a retrospective cohort study revealed that an elevated AGEs/RAGE ratio was associated with increased mortality risk in patients with type 2 diabetes.[16] Subsequently, numerous studies have explored interventions to prevent and treat AGEs-RAGE-induced damage by blocking the AGEs-RAGE interaction. Finding effective AGEs-RAGE axis inhibitors is a promising approach to reduce endothelial injury.[17]

Heparin is a linear, heterogeneous, highly sulfated, anionic glycosaminoglycan complex.[18,19] Despite its wide use in clinical settings as an anticoagulant, its complex structure and diverse components offer untapped potential for alternative applications.[20] In addition to its well-established anticoagulant effects, heparin has been shown to have additional effects specifically with respect to inhibition of angiogenesis and neovascularization. This mechanism is thought to involve heparin sequestrating angiogenic growth factors (AGF) in the extracellular

[1]Department of Endocrinology and Metabolism, Affiliated Hospital of Shandong Second Medical University, Weifang, China
[2]Clinical Research Center, Affiliated Hospital of Shandong Second Medical University, Weifang, China
[3]School of Stomatology, Henan University, Kaifeng, Henan, China
[4]Department of Oncology, Affiliated Hospital of Shandong Second Medical University, Weifang, China
[5]Department of Pathology, Affiliated Hospital of Shandong Second Medical University, Weifang, China
[6]Department of Hepatobiliary and Pancreatic Surgery, Affiliated Hospital of Shandong Second Medical University, Weifang, China
[7]Medical Research Center, The Affiliated Hospital of Qingdao University, 16 Jiangsu Road, Qingdao, P.R. China
[8]These authors contributed equally
[9]Lead contact
*Correspondence: xiaodong.sun@sdsmu.edu.cn (X.S.), qiuhongyan@sdsmu.edu.cn (H.Q.)
https://doi.org/10.1016/j.isci.2024.111084

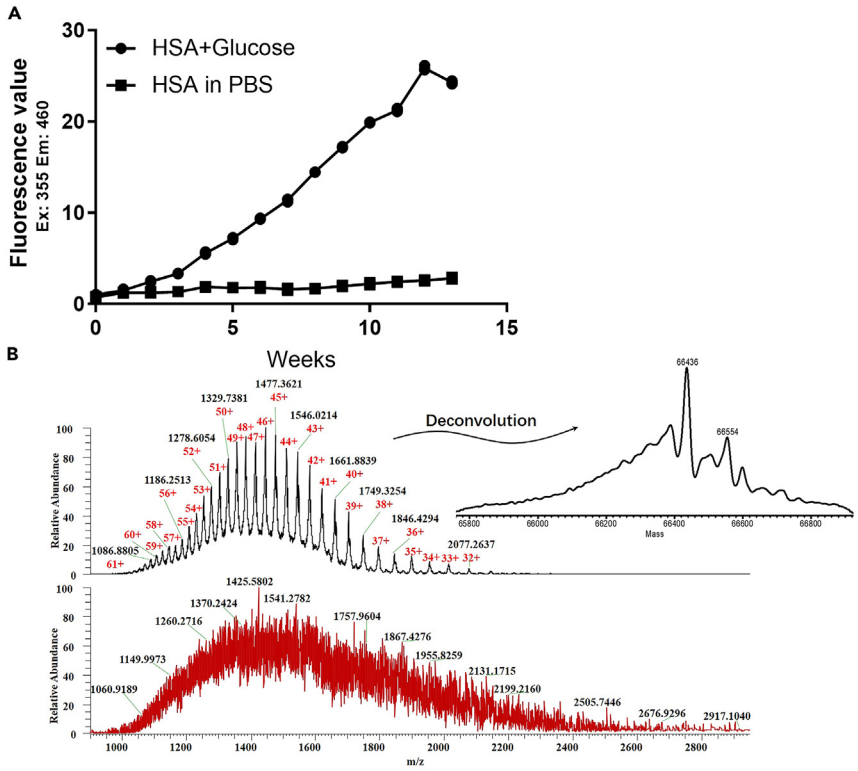


**Figure 1. AGEs preparation and analysis**

(A) Fluorescence was measured weekly during reactions of HSA with PBS or glucose.

(B) LC-MS spectra of HSA and AGEs and the deconvolution spectrum of HSA. The molecular weight of the deconvolved HSA was 66,436 Da, and the AGEs molecules could not be deconvolved.

environment and impeding the interaction between AGF and extracellular matrix-proteoglycans.[21] While this may be beneficial in protecting against tumorigenesis,[22] it can have negative effects in certain pediatric conditions (e.g., pulmonary hypoplasia) in which survival depends on growth and angiogenesis.[23]

In recent years, interest in the anti-inflammatory properties of heparin has increased.[24] For instance, heparin has demonstrated efficacy in reducing disease progression and necrosis rates in severe pancreatitis through its anti-inflammatory effects.[25] Pan et al. reported that the anti-inflammatory effect of heparin is related to its non-anticoagulant structure.[26] This anti-inflammatory activity also extends to sepsis and plays a crucial role in safeguarding endothelial integrity.[27] Additionally, low-molecular-weight heparin (LMWH) has been shown to inhibit the interaction between AGEs and RAGE in diabetes-associated kidney failure and diabetic endothelium damage.[24,28] This effect is thought to be related to the fact that RAGE has been reported to act as a receptor for specific sulfated glycosaminoglycans.[29] Glycosaminoglycans such as heparin compete with AGEs for binding with RAGE, thereby blocking the inflammatory response triggered by the AGEs-RAGE axis. Furthermore, an important consideration is that in *in vivo* state heparin exerts many of its roles through the interaction of conserved heparin-binding domain with multiple proteins in the extracellular matrix, including involvement in cell attachment, migration, invasion, inflammation, and injury responses.[30,31] Nevertheless, further studies are needed to fully understand the molecular mechanisms underlying the effects of heparin on endothelial cells in the diabetic state.

In this study, we explored the protective potential of heparin against AGEs-stimulated endothelial cells. Our investigation included qualitative and quantitative analyses of the impact of heparin on AGEs-stimulated endothelial cells through proteomic analysis and cell biology experiments. In addition, a diabetic mouse model was used to confirm relevant changes in proteomic and biological processes. Our findings provide compelling evidence that heparin has the capacity to ameliorate AGEs-induced damage in endothelial cells.

## RESULTS

### Formation of AGEs through glucose and human serum albumin

AGEs was prepared using human serum albumin (HSA) and glucose and a negative control was established using HSA-PBS. The fluorescence values of AGEs were recorded weekly. Notably, the fluorescence of HSA in glucose and PBS at week 0 was close to zero. As the reaction time increased, fluorescent AGEs gradually formed in the presence of glucose, with the peak value occurring at week 12. In contrast, the fluorescence value of HSA-PBS did not significantly change from week 0 to week 13 (Figure 1A).

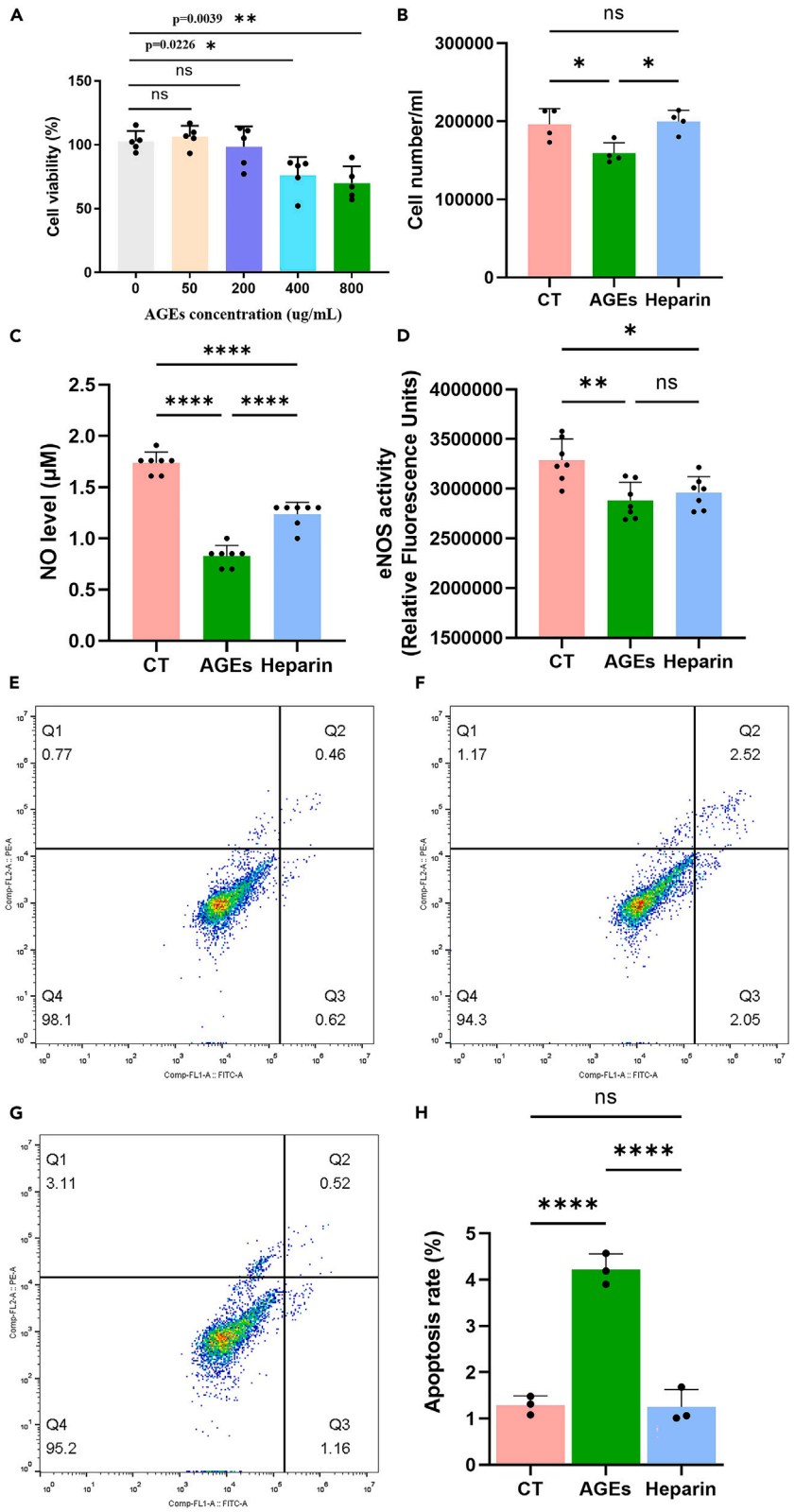
A
p=0.0039 **
p=0.0226 *
ns
ns
Cell viability (%)
150
100
50
0
0
50
200
400
800
AGEs concentration (ug/mL)
B
ns
*
*
Cell number/ml
300000
200000
100000
0
CT
AGEs
Heparin
C
****
****
****
NO level (μM)
2.5
2.0
1.5
1.0
0.5
0.0
CT
AGEs
Heparin
D
*
**
ns
eNOS activity (Relative Fluorescence Units)
4000000
3500000
3000000
2500000
2000000
1500000
CT
AGEs
Heparin
E
Q1
0.77
Q2
0.46
Q4
98.1
Q3
0.62
Comp-FL2-A :: PE-A
Comp-FL1-A :: FITC-A
F
Q1
1.17
Q2
2.52
Q4
94.3
Q3
2.05
Comp-FL2-A :: PE-A
Comp-FL1-A :: FITC-A
G
Q1
3.11
Q2
0.52
Q4
95.2
Q3
1.16
Comp-FL2-A :: PE-A
Comp-FL1-A :: FITC-A
H
ns
****
****
Apoptosis rate (%)
5
4
3
2
1
0
CT
AGEs
Heparin

**Figure 2. Heparin ameliorates the biological and biochemical damage caused by AGEs stimulation**

(A) Changes in cell viability in response to 0, 50, 200, 400, and 800 μg/mL AGEs.

(B) Changes in cell number/mL in response to 800 μg/mL AGEs and 800 μg/mL AGEs +200 μg/mL heparin ($n$ = 5).

(C) Changes in NO levels in response to 800 μg/mL AGEs and 800 μg/mL AGEs +200 μg/mL heparin ($n$ = 4).

(D) Changes in eNOS activity in response to 800 μg/mL AGEs and 800 μg/mL AGEs +200 μg/mL heparin ($n$ = 7).

(E–G) Cell apoptosis in each group was analyzed by flow cytometry; E is the CT group, F is the AGEs group, and G is the heparin group. Q1 represents nude cells; Q2 represents late apoptotic or necrotic cells; Q3 represents early apoptotic cells; and Q4 represents living cells.

(H) Changes in the percentage of apoptotic cells in each group ($n$ = 3). For all experiments, the data are presented as means ± SDs (ns, $p > 0.05$; *, $p < 0.05$; **, $p < 0.01$; ***, $p < 0.001$; ****$p < 0.0001$, all by ordinary one-way ANOVA [multiple comparisons]).

Liquid chromatography (LC)-mass spectrometry (MS) was used to analyze HSA at week 12. Interestingly, in the absence of glucose, the monoisotopic peak of HSA was clearly distinguishable, displaying a regular sine wave pattern. The monoisotopic peak was deconvoluted to calculate exact molecular weight, revealing a 66,436 Da for HSA derived from PBS. However, the molecular weight of HSA derived from glucose could not be calculated. This discrepancy is likely due to the formation of complex AGE compounds through the glycation of HSA, making them indistinguishable by deconvolution (Figure 1B). This observation strongly supports the successful preparation of AGEs and indicates cross-linking between HSA and the secondary and end-product AGEs generated during the glucose reaction.

## Heparin mitigates AGEs-induced endothelial cell damage

HUVECs were stimulated with 0, 50, 200, 400, or 800 μg/mL AGEs, resulting in a decrease in cell viability as the AGEs concentration increased. Specifically, 800 μg/mL AGEs ($p$ = 0.0039) had a significantly greater impact than 0 μg/mL AGEs (Figure 2A). Consequently, 800 μg/mL AGEs was chosen to stimulate HUVECs. Changes in cell number, NO level and eNOS activity were assessed (Figures 2B–2D). After AGEs stimulation, all three indicators (cell number: $p$ = 0.0267, NO level: $p < 0.0001$ and eNOS activity: $p$ = 0.0023) decreased significantly. Following heparin intervention, the cell number ($p$ = 0.0162) and NO concentration ($p < 0.0001$) increased significantly, while eNOS activity tended to increase, although the increase was not statistically significant. Additionally, flow cytometry was used to detect early and late apoptotic cells. The rate of apoptosis increased 2.3-fold after AGEs stimulation compared to that in the CT group ($p < 0.0001$), but it decreased to a level similar to that in the CT group after heparin intervention (Figures 2E–2H).

The permeability of endothelial cells was also evaluated by adding FITC-BSA after different treatments and using confocal microscopy to detect fluorescence localization (Figure S1). Under the stimulation of AGEs, the degree of cell damage increased, with obvious green fluorescence. After heparin treatment, endothelial cell damage and permeability were reduced in the heparin group compared to the AGEs group, and tended to be consistent with the CT group. These comprehensive findings indicate that AGEs induce pathological changes in HUVECs but that those changes can be ameliorated by heparin intervention.

## Heparin antagonizes the AGEs-RAGE axis, reducing inflammatory factor

Immunofluorescence labeling unveiled a widespread distribution of RAGE on the cell surface. The fluorescence intensity of RAGE was significantly higher in the AGEs group than in the CT group ($p < 0.0001$). However, it notably decreased following heparin intervention ($p$ = 0.0108) (Figures 3A and 3B). This observation supports the activation of RAGE on the cell surface by AGEs and its inhibition by heparin.

To validate these findings, we examined RAGE expression at both the gene and protein levels. RAGE mRNA expression increased after AGEs stimulation ($p$ = 0.0018) but decreased after heparin intervention ($p$ = 0.0006) (Figure 3C). Western blotting results also demonstrated that RAGE protein expression was upregulated following AGEs stimulation ($p$ = 0.0119) and downregulated after heparin intervention ($p$ = 0.0102), with no significant difference compared to the CT group (Figures 3D and 3E). These results collectively indicate that AGEs activate both intracellular and extracellular RAGE, while heparin inhibits the interaction between AGEs and RAGE.

Furthermore, we investigated changes in the inflammatory factor NF-κB. The results showed that NF-κB expression increased in response to AGEs ($p$ = 0.0203) and decreased after heparin intervention ($p$ = 0.0041) (Figures 3D and 3F). This finding confirmed that AGEs bind to its receptor RAGE and activate the downstream NF-κB signaling pathway, further increasing RAGE levels in cells and accelerating cell damage, while heparin inhibited the AGEs-RAGE-NFκB signaling axis, attenuating inflammatory responses.

## Proteomic analysis reveals differential protein expression induced by AGEs and heparin

Proteomics was used to analyze the molecular changes induced by AGEs and heparin. A total of 9174 proteins were identified. 268 proteins differentially expressed between the AGEs group and CT group, of which 129 were upregulated and 139 were downregulated (Figure S2A). Furthermore, 440 differentially expressed proteins were identified between the heparin group and the AGEs group, including 168 upregulated and 272 downregulated proteins (Figure S2B). Notably, 187 and 359 proteins were unique and 81 proteins were coexpressed in the AGEs/CT and heparin/AGEs groups, respectively (Figure 4A). To further understand whether the above 81 proteins are related to DM, the online mendelian inheritance in man (OMIM) and genecards databases were searched. fifty-three proteins associated with diabetes were identified (Table S1). The results further verified that most of the differential proteins screened by proteomic analysis existed in diabetic proteins. Additionally, some proteins that were only present in one group were also important, as detailed in Table S2. Combined with the 81 coexpressed proteins resulted in a total of 121 differentially proteins.

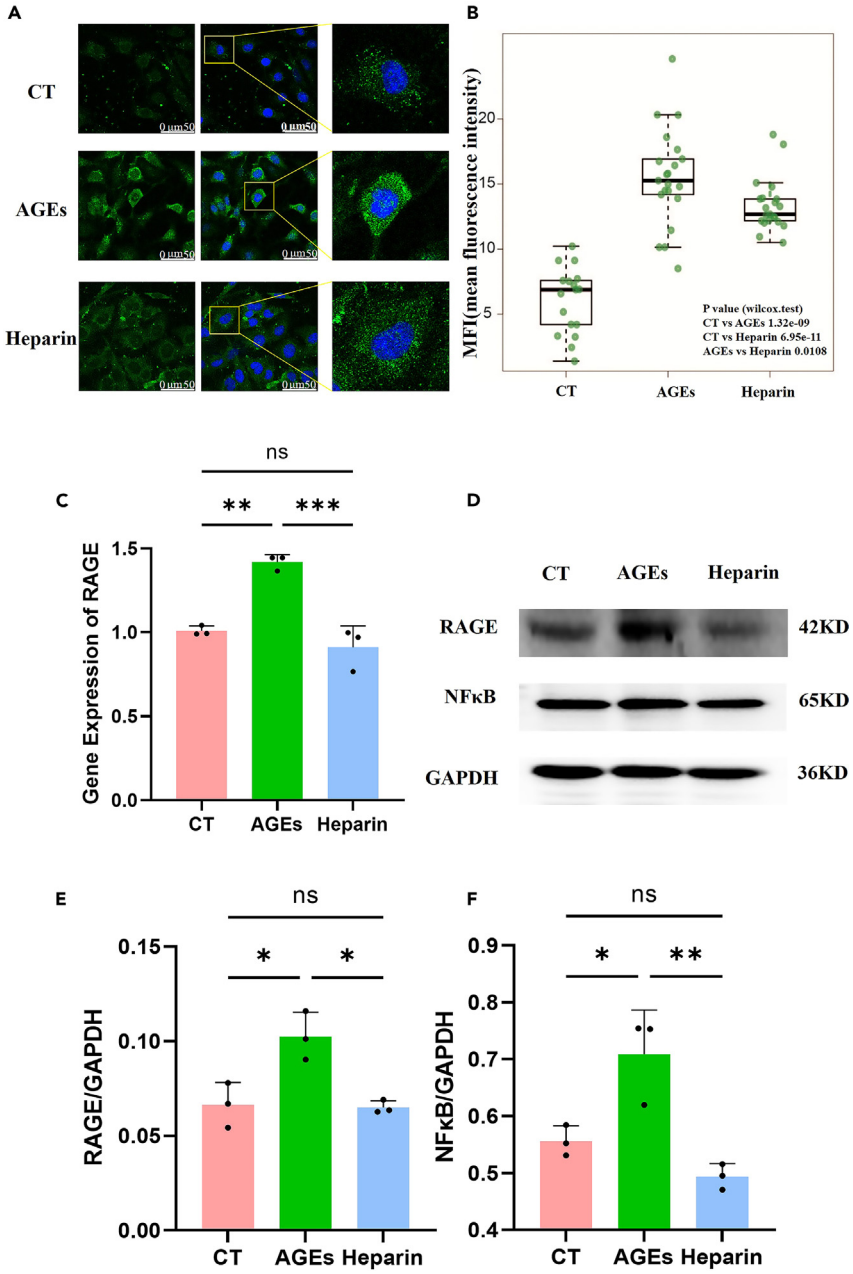


**Figure 3. Heparin inhibits the AGEs-RAGE axis**

(A) Immunofluorescence of RAGE in the CT group, 800 μg/mL AGEs group and 800 μg/mL AGEs +200 μg/mL heparin group.

(B) MFI (mean fluorescence intensity) of the three groups.

(C) mRNA levels of RAGE in the three groups ($n = 3$).

(D–F) Immunoblotting analysis and quantification of RAGE and NF-κB ($n = 3$). The data are presented as means ± SDs (ns, $p > 0.05$; *, $p < 0.05$; **, $p < 0.01$; ***, $p < 0.001$; all by ordinary one-way ANOVA [multiple comparisons]).

Gene ontology (GO) annotation was performed to evaluate the functional significance of the 121 differentially expressed proteins. The top 20 biological processes encompassed proteins involved in nucleic acid and biomacromolecule-mediated reactions, including processes such as "protein modification", "regulation of macromolecule biosynthesis", "macromolecule modification", "response to stress" and "regulation of gene expression" (Figure S3A). The top 20 cellular components included "nucleolus", "organelle membrane", "plasma membrane-bound cell projection", "integral component of membrane" and "protein-containing complex" (Figure S3B), indicating the involvement of these differentially expressed proteins in various intracellular structures. Additionally, the top 20 molecular functions included "carbohydrate

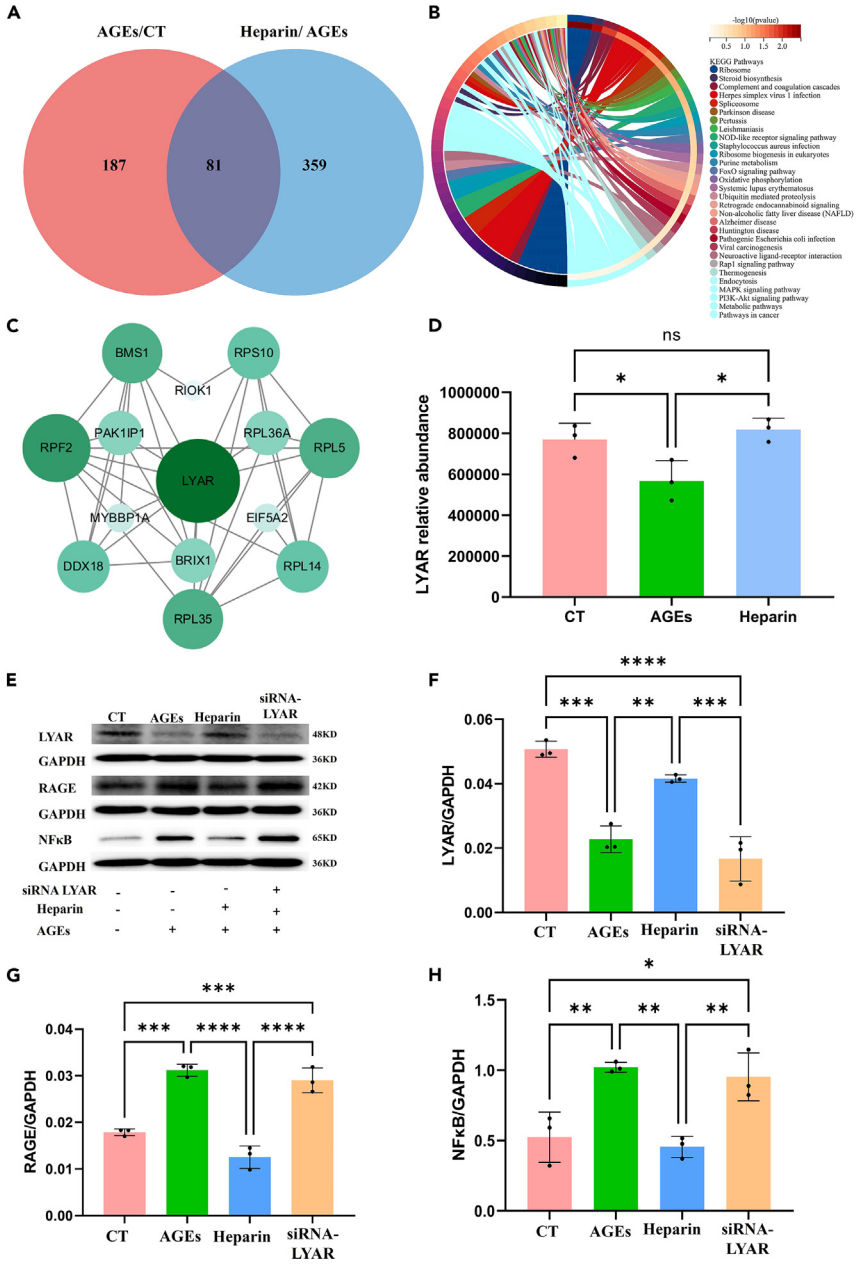


**Figure 4. Changes in the intracellular proteome in response to heparin and AGEs**

(A) Venn diagram of enrichment in the AGEs/CT groups and heparin/AGEs groups (red and blue).

(B) KEGG pathways of differentially expressed proteins between the AGEs/CT group and the heparin/AGEs group.

(C) PPIs of the major differentially expressed proteins in the AGEs/CT and heparin/AGEs groups.

(D) Comparison of LYAR in proteomic quantitative results.

(E–H) Immunoblot analysis and quantification of LYAR ($n$ = 3), RAGE ($n$ = 3), and NF-κB ($n$ = 3) in CT, AGEs, Heparin, and siRNA-LYAR groups. (ns, $p > 0.05$; *, $p < 0.05$, **, $p < 0.01$; ****, $p < 0.001$; all by ordinary one-way ANOVA (multiple comparisons)).

derivative binding", "catalytic activity, acting on a protein", "drug binding", "molecular function regulator" and "enzyme binding" most of which were related to proteins and carbohydrates and closely associated with AGEs (Figure S3C).

Subsequently, Kyoto encyclopedia of genes and genomes (KEGG) enrichment analysis was performed on the 121 identified differentially expressed proteins to determine their biological functions (Figure 4B). The results revealed enrichment in pathways such as "ribosome", "Parkinson's disease", "oxidative phosphorylation", "MAPK signaling", "PI3K-Akt signaling pathway", "mTOR (mechanistic target of

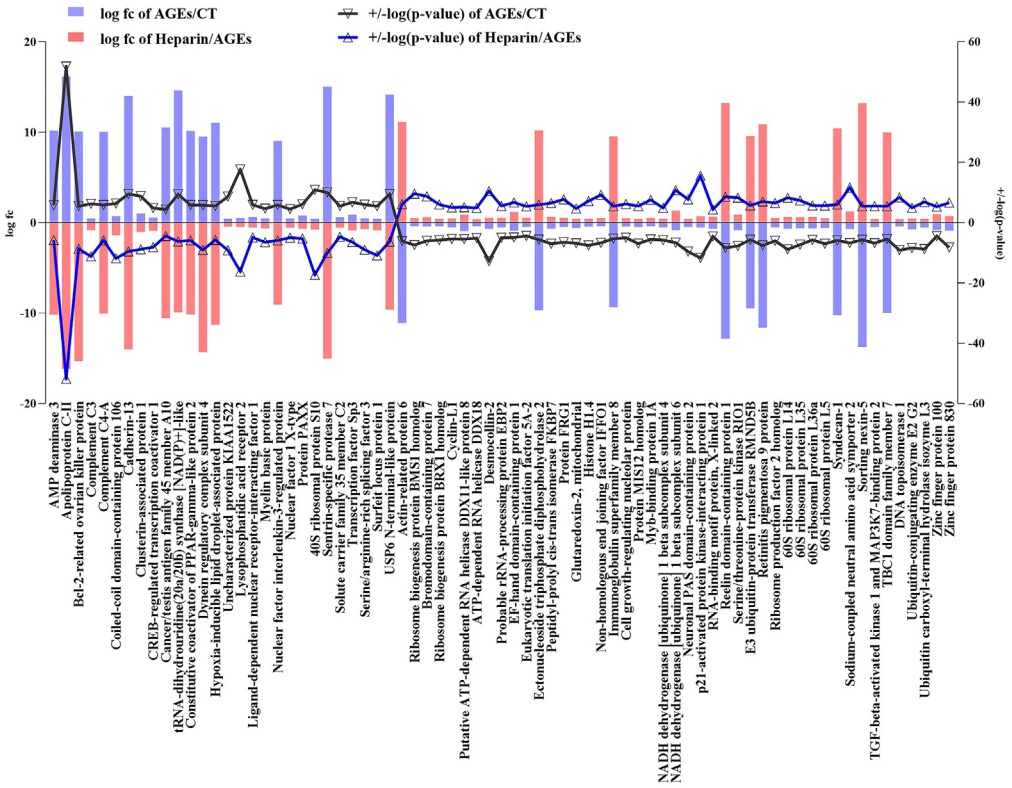


**Figure 5. Proteins with opposite expression trends in the AGEs/CT and heparin/AGEs groups**

Downregulated proteins in the AGEs/CT group are represented in purple, and those in the heparin/AGEs group are represented in pink. The black solid line represents the ±log (*p* value) change in protein expression in the AGEs/CT groups, and the blue line represents the ±log (*p* value) change in protein expression in the heparin/AGEs groups. In the left panel, the y axis is the value of the log-fold change, and in the right panel, y axis is the ±log (*p* value).

rapamycin ) signaling pathway", "autophagy-animal", "AMPK (AMP-activated protein kinase)pathway", "TNF (tumor necrosis factor) signaling pathway", "NF-κB signaling pathway" and "IL (Interleukin) -17 signaling pathway" which are linked to inflammation and autophagy pathways (Table S3).

## Protein interaction analysis and verification

Oppositely expressed proteins between the AGEs/CT and heparin/AGEs groups and proteins expressed under only one of the treatments were used for protein interaction analyses. A protein-protein interaction (PPI) network was constructed via the STRING database (Figure 4C). Notably, the cell growth-regulating nucleolar protein LYAR had the most interactions and was a key node in the PPI network. Combined with the quantitative results of proteomics, LYAR expression decreased following AGEs stimulation ($p = 0.0499$) and increased after heparin intervention ($p = 0.0206$) (Figure 4D). Subsequently, western blotting was used to verify the expression of LYAR and explore its importance. The results demonstrated decreased LYAR expression following AGEs stimulation ($p = 0.0002$) and increased LYAR expression after heparin intervention ($p = 0.0028$) (Figures 4E and 4F). The expression trend of RAGE and NF-κB was opposite to that of LYAR (Figures 4E, 4G, and 4H). LYAR is a nucleolar protein that regulates cell growth and inflammation. To further investigate the importance of LYAR, the knockdown experiment was performed at the cellular level. Compared with the heparin group, the protective effect of heparin was ineffective in the LYAR knockdown group (Figures 4E–4H). This result demonstrated that LYAR knockdown would affect the AGEs-RAGE- NF-κB axis and further increase the degree of inflammation.

## Changes in the molecular regulation induced by AGEs and heparin

To understand the specific regulatory changes associated with the differentially expressed proteins, the upregulation and downregulation of 81 differentially expressed proteins in the AGEs/CT and heparin/AGEs groups were compared, as detailed in Table S4. Notably, 74 proteins exhibited opposite expression trends (Figure 5). The expression of some proteins, including "complement C3", "complement C4-A", "clusterin-associated protein 1", "40S ribosomal protein S10" and "apolipoprotein C-II", was upregulated in response to AGEs but downregulated following heparin intervention. AGEs activate complement to mediate the development of stress, whereas heparin inhibits the activation of related proteins. Proteins for which the expression was downregulated by AGEs and upregulated by heparin intervention included "cell

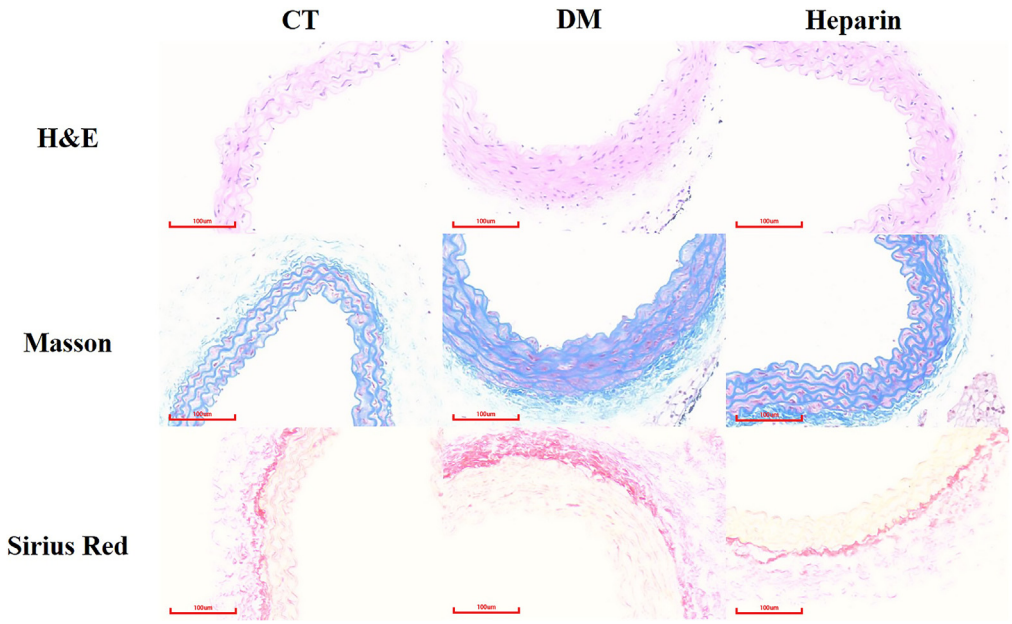


**Figure 6. Pathological changes in mouse blood vessels under different interventions**

In the H&E-stained sections, the nucleus is blue, and the cytoplasm is red. In the Masson's trichrome-stained sections, collagen fibers are blue, and muscle fibers are purplish red. In the Sirius red-stained sections, collagen fibers are red with a yellow background, and type I collagen fibers are orange or bright red thick fibers.

growth-regulating nucleolar protein", "Myb-binding protein 1A", "ATP-dependent RNA helicase DDX18", "serine/threonine-protein kinase RIO1", "ribosome production factor 2 homolog", and "TGF-beta-activated kinase 1 and MAP3K7-binding protein 2". These proteins are involved in cell growth, immunity, and energy metabolism, further indicating that the normal physiology of cells was inhibited by AGEs and that the inhibition of AGEs was ameliorated by heparin.

### Vascular endothelial fibrosis and related molecular validation in mice

The results of the cell experiments confirmed that heparin improved AGEs-induced endothelial cell damage. On this basis, C57BL/6J mice were subjected to further intervention to observe the changes in vascular tissue. Some diabetic mice experienced side effects (subcutaneous hemorrhage at the injection site, ecchymosis diameter less than 1 cm) after heparin injection. HE (hematoxylin-eosin) staining revealed irregular thickening of the basement membrane and arterial media in DM mice. After heparin intervention, the state of vascular thickening normalized (Figure 6). In addition, compared with that in the CT group, vascular fibrosis in the DM group was aggravated, with evidence of severe hyperplasia of fibers in the membranes of arteries after Masson staining (Figure 6). Sirius red staining revealed that the proliferative fibers were mainly type I collagen fibers with disordered structures. In contrast, the degree of fibrosis decreased after heparin intervention (Figure 6).

The relationship between heparin and the core protein LYAR was further analyzed, and changes in the expression of the vascular marker CD31 and the inflammatory factor NF-κB were also observed (Figure 7). The immunohistochemistry results for the vascular endothelium showed that CD31 and LYAR staining was weak in DM mice but increased in intensity after heparin administration (Figure 7A). The proportion of these positive cells was significantly lower in DM than that of CT group (CD31, $p = 0.0332$; LYAR, $p = 0.0282$) (Figure 7B). Both of these parameters normalized after heparin intervention (CD31, $p = 0.0299$; LYAR, $p = 0.0161$), but there was no significant difference compared with those in the CT group (CD31, $p = 0.9957$; LYAR, $p = 0.8793$) (Figure 7B). In contrast, NF-κB content increased in the whole vascular endothelial cell layer in the DM group, and the proportion of positive cells was greater than that in the CT group ($p = 0.0123$) (Figure 7B). Heparin reversed NF-κB activation ($p = 0.0251$) (Figure 7B). Western blotting was also used to further verify the changes in LYAR and NF-κB protein expression in mouse vascular tissues. LYAR protein expression was downregulated in the DM group ($p = 0.0298$) and upregulated in the heparin group ($p = 0.0206$) (Figures 7C and 7E). Moreover, the protein expression of NF-κB was increased in the DM group ($p = 0.0156$), an effect that was inhibited by heparin treatment ($p = 0.0237$) (Figures 7D and 7F).

## DISCUSSION

This study explored the potential protective effects of heparin against AGEs-induced endothelial damage, primarily through its anti-inflammatory properties. AGEs, the products of glycation, are known to trigger inflammatory responses, disrupt vascular endothelial homeostasis, and contribute to microvascular and macrovascular complications in diabetes.[13,16] In this investigation, AGEs were generated by reacting glucose and HSA, and the complex structural changes were subsequently revealed by LC-MS analysis. By week 12, the fluorescence value

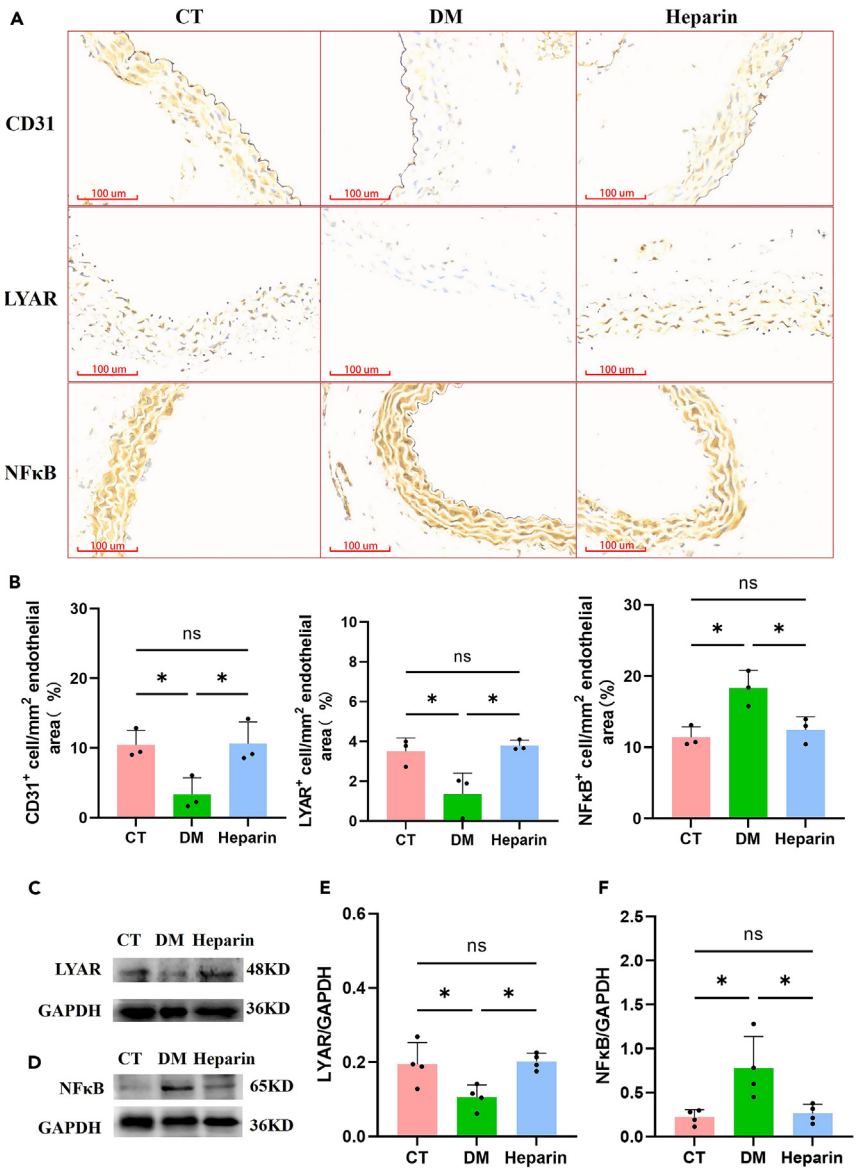


**Figure 7. Molecular mechanisms for ameliorating vascular injury**

(A) Immunohistochemical results for CD31, LYAR, and NF-κB.

(B) Area ratio of positive cells to endothelial cells ($n$ = 3).

(C–F) Immunoblot analysis and quantification of LYAR and NF-κB content ($n$ = 4). (ns, $p > 0.05$; *, $p < 0.05$, all by ordinary one-way ANOVA [multiple comparisons]).

reached 26 au, and the MS data could not be deconvolved to determine the exact molecular mass. This complexity likely arises from the dehydration, rearrangement, and cross-linking of glycation products, which alter their structure and function.[32] In contrast, non-glycated HSA retained an exact molecular weight of 66,436 Da, indicating that AGEs were successfully generated through nonenzymatic glycation.

Subsequently, cell viability was assessed to determine the degree of damage to HUVECs induced by different concentrations of AGEs. Notably, the lowest cell viability was observed at a concentration of 800 μg/mL. The apparent changes in cell biology further confirmed that the cellular damage caused by AGEs stimulation can manifest through multiple pathways. On the one hand, cell number and NO and eNOS activities are decreased; NO formation caused by eNOS is the core process regulating vascular homeostasis.[33] The impairment of NO production, a key regulator of vascular function, further highlights the detrimental effects of AGEs.[33,34] However, eNOS activity was less affected, possibly due to the complex enzymatic mechanisms involved. On the other hand, the flow cytometry data and cell permeability experiment showed elevated apoptotic cells and cell permeability after stimulation with AGEs. Intriguingly, in the presence of heparin, cell numbers, NO levels and eNOS activity increased, while the apoptosis and permeability decreased. This collective evidence underscores the ameliorative effect of heparin on AGEs-induced cellular damage.

AGEs exert their effects intracellularly by binding to the receptor RAGE, which is widely expressed on various cell types.[12] Scanning electron microscopy showed that RAGE fluorescence increased after AGEs stimulation and that was mitigated after heparin intervention. This observation was also validated at the gene and protein levels, i.e., AGEs increased the expression of RAGE and NF-κB, enabling the sustained maintenance of inflammatory events. This finding is consistent with the findings of Wu et al. that AGEs binding to RAGE induces the activation of chronic oxidative stress-related inflammatory molecules such as NF-κB, PI3K/AKT, and MAPK/ERK.[10] In contrast, with the intervention of heparin, inflammation-induced cell damage was alleviated, as shown by the decrease in RAGE and NF-κB protein expression, which was similar to that in normal cells.

To further understand how heparin protects HUVECs, we employed nanoLC-MS/MS to analyze the cellular proteome, identifying 9,174 proteins across the three experimental groups. Among them, there were proteins with upregulated and downregulated expression between the AGEs-treated group and the CT group. In the comparison between heparin and AGEs group, there were also proteins with upregulated and downregulated expression. Ensemble analysis revealed that 81 proteins were coexpressed between the AGEs/CT groups and heparin/AGE groups. These 81 proteins combined with proteins that were only present in one group were subjected to GO and KEGG enrichment analysis. GO analysis revealed that AGEs and heparin affected the expression of macromolecules such as proteins and nucleic acids and the biological functions related to the stress response; the structure of the cell membrane, cytoplasm, organelle and nucleus; and molecular functions such as the binding of proteins, carbohydrates and drugs etc. In addition, KEGG enrichment analysis showed that these differentially expressed proteins were enriched in signaling pathways involving inflammatory factors, chemokines and autophagy factors, which are related to the inflammatory process. The specific pathways and molecules included oxidative phosphorylation, NF-κB, MAPK, PI3K-Akt, mTOR, AMPK, and TNF. These molecules are enriched as downstream activators of RAGE that participate in intracellular activities.[35] Guglielmo et al. confirmed that RAGE stimulates Akt, MAPK, and JNK in endothelial cells, chondrocytes, macrophages/monocytes/microglia, astrocytes, and vascular smooth muscle cells, leading to cellular activation and/or proliferation in atherosclerosis and/or inflammation and arthritis.[12]

Further analysis revealed that 28 proteins, such as complement-related proteins, apolipoproteins and clusterin-associated proteins, increased after AGEs stimulation but decreased after heparin intervention. These results further suggest that AGEs and heparin may mediate complement activation and inhibition. The expression of 45 proteins, such as ribosomes, Myb-binding proteins and growth-related proteins, decreased in response to AGEs stimulation but increased in response to heparin intervention. The changes in protein levels indicated that AGEs and heparin may affect ribosome assembly and cell growth. Regarding the interactions between proteins, there were 14 nodes in the PPI network. The molecule LYAR, located at the center of the network and involved in ribosome biosynthesis, is a nucleolar protein with a zinc finger DNA binding sequence and plays a vital role in cell growth and proliferation.[36] Naoki et al. found that LYAR functions by acting on 32S, 47S/45S, 30S, and 21S preribosomes and that LYAR overexpression increases cell proliferation and occurs in some rapidly growing cells.[37] Western blotting analysis verified that LYAR expression decreased after AGEs stimulation and normalized after heparin treatment. LYAR knockdown experiments showed that the protective effect of heparin was ineffective in the LYAR knockdown state, which was manifested in the increase of RAGE and NF-κB, indicating that LYAR was involved in the regulation of AGEs-RAGE- NF-κB. However, whether LYAR lowers NF-κB by inhibiting RAGE or reduces RAGE by inhibiting NF-κB requires further research to determine the underlying mechanism.

HE, Masson's trichrome and Sirius red staining showed that diabetes caused vascular basement membrane thickening, vascular fibrosis, and increased type I collagen, that are consistent with previous studies.[38–40] However, these changes improved after heparin injection. Vascular immunohistochemistry showed that CD31 and LYAR levels were significantly decreased in the DM group but normalized in the heparin group. However, the inflammatory factor NF-κB showed the opposite trend to that of CD31 and LYAR in the DM group, and this effect was reversed by the administration of heparin. Western blotting analysis further verified the changes in LYAR and NF-κB at vascular tissues.

The immunohistochemistry and western blot results confirmed that heparin upregulated LYAR and downregulated NF-κB to alleviate inflammation and injury to vascular tissue in DM mice. Combined with the LYAR knockdown experiment, our results are consistent with the Cha Yang's study, which confirmed that LYAR inhibits NFκB-mediated expression of pro-inflammatory cytokines.[41] Therefore, another reason why heparin reduces NF-κB may be that heparin increases LYAR expression and thus inhibits NF-κB damage.

In summary, these findings highlight the potential of heparin to promote the recovery of damaged endothelium while mitigating AGEs-induced injury at deep levels. As shown in Figure 8, with increasing glucose concentration in the blood, the amino groups of proteins react with glucose to generate AGEs. AGEs bind to the receptor RAGE on the surface of vascular endothelial cells to activate the NADPH oxidase ROS, which in turn activates ERK, MAPK, and AKT. Finally, NF-κB is activated, leading to decreased NO and eNOS levels, increased autophagy, apoptosis, immune disorders, and ultimately vascular endothelial tissue damage. However, in the presence of heparin, endothelial cell damage is less severe. Heparin was used as traditional anticoagulants, has been reported to interact with many biologically related proteins in recent years, leading to the discovery of many additional anti-viral, anti-tumor, anti-inflammatory, and anti-angiogenesis activities.[18] Heparin inhibits the AGEs-RAGE axis mainly through the following three targets: firstly, it has been reported that RAGE can serve as a receptor for specific sulfated glycosaminoglycans,[29] while heparin, as a class of glycosaminoglycans, can competitively bind to RAGE, thereby inhibiting the interaction between AGEs and RAGE.[24] Secondly, multiple literature reports suggest that heparin exerts its effects through conserved binding domains and interactions with various inflammatory proteins in the extracellular matrix.[30,31] Thirdly, it has been broadly reported that heparin interacts with HMGB-1 to interface with RAGE associated signaling pathway.[42] Heparin interferes with AGEs-RAGE-NFκB axis through previous various mechanisms, including upregulated LYAR, thereby offering a protective role against AGEs-induced damage.

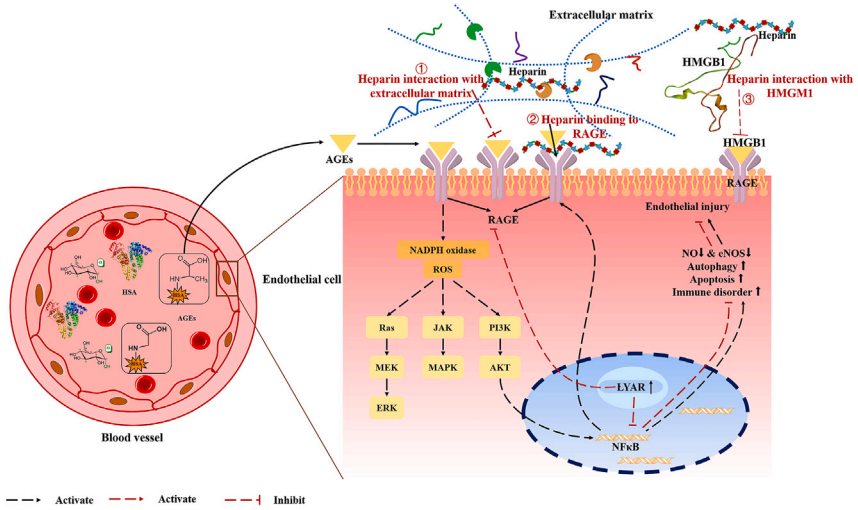


**Figure 8. Heparin enhances recovery after AGEs-stimulated endothelial injury**

The combination of glucose and proteins in the blood generates AGEs, which bind to RAGE on the membrane of vascular endothelial cells to activate NADPH and ROS, inducing downstream signaling pathways, such as the Ras-MEK-ERK/JAK-MAPK/PI3K-AKT pathways, to mediate inflammation. AKT activates the nuclear expression of NF-κB, which exacerbates inflammation and injures vascular endothelial cells. However, heparin antagonizes the AGEs-RAGE interaction by competitively binding RAGE, and interaction with extracellular matrix proteins or HMGB-1 to block RAGE signaling pathway. Additionally, heparin promotes the expression of LYAR, ultimately alleviating vascular endothelial injury.

## Conclusion

This study demonstrates the protective effects of heparin against AGEs-induced endothelial cell dysfunction. Heparin significantly antagonized AGEs-induced decreases in eNOS activity and NO levels, increased cell proliferation, and attenuated cell apoptosis. It interrupts the cascade initiated by the AGEs-RAGE axis, reducing the expression of downstream inflammatory signaling molecules. Furthermore, alterations in cellular proteins serve as a direct response to AGEs-induced damage and the ameliorative effects of heparin. This encompasses processes such as DNA binding, RNA modification, protein posttranslational modifications, ribosome assembly and perturbations in key signaling pathways, such as the NF-κB, PI3K, and MAPK pathways. In particular, heparin modulated the expression of nucleolar growth regulatory proteins-LYAR in DM state, ultimately governing the recovery of impaired endothelial cells through decrease of RAGE and NF-κB. This comprehensive elucidation not only deepens our understanding of the pathogenesis underlying microvascular and macrovascular complications in diabetes but also extends our knowledge of cellular biology and molecular mechanisms under AGEs stimulation. An innovative concept explored herein involves the subdivision of the complex structure of heparin to selectively eliminate its anticoagulant components while retaining its anti-inflammatory properties. This strategy could pave the way for developing new therapeutic approaches and drug formulations to combat diabetes and its complications.

## Limitations of the study

This study has some limitations. First, because heparin has a complex structure, it is essential to subdivide the complex structure of heparin to further investigate the role of each component in the protection of diabetic endothelium. Second, an important consideration is that heparin exerts many of its roles *in vivo* through its interaction with extracellular matrix, and the extracellular matrix component was not involved in this study, inclusion of the extracellular matrix component in future studies is necessary. In addition, the mechanism by which heparin restores LYAR expression in diabetes and whether LYAR lowers NF-κB by inhibiting RAGE or reduces RAGE by inhibiting NF-κB requires further research to determine the underlying mechanism.

# RESOURCE AVAILABILITY

## Lead contact

Further information and requests for resources and reagents should be directed to Hongyan Qiu at Qiuhongyan@sdsmu.edu.cn.

## Materials availability

This study did not generate new unique reagents.

## Data and code availability

- The datasets presented in this study can be found in iProX integrated proteome resources (IPX0009808000).

- This article does not report the original code.
- Any additional information required to reanalyze the data reported in this article is available from the lead contact upon request.

## ACKNOWLEDGMENTS

This work was supported by the Natural Science Foundation of Shandong Province of China (ZR2022QH013, ZR2021QD132, ZR2020MH106, ZR2020QH286), National Natural Science Foundation of China (82170865, 82370856); Weifang Science and Technology Development Plan Project (2023YX047); Taishan Scholars Project of Shandong Province (tsqn202211365) and Public Domestic Visiting Program of Weifang Medical University.

## AUTHOR CONTRIBUTIONS

J.S.: software, methodology and formal analysis. Y.G.: data curation and methodology. H.S.: writing original draft. L.Z., J.L., Q.L., M.S., K.Z., and M.W.: validation, visualization and investigation. N.H., F.H., X.S., and H.Q.: conceptualization, project administration, supervision and writing—review and editing.

## DECLARATION OF INTERESTS

The authors have no conflict of interest.

## STAR★METHODS

Detailed methods are provided in the online version of this paper and include the following:

- KEY RESOURCES TABLE
- EXPERIMENTAL MODEL AND STUDY PARTICIPANT DETAILS
  - Cells
  - Mice
- METHOD DETAILS
  - AGEs preparation and analysis
  - Measurement of cell viability in response to AGEs stimulation
  - Cell biological and biochemical assays
  - Immunofluorescence
  - Western blotting
  - Reverse transcription polymerase chain reaction analysis
  - LC-MS/MS analysis
  - Cell transfection experiments
  - Animals experimental
  - Histopathological and immunohistochemical analysis
- QUANTIFICATION AND STATISTICAL ANALYSIS

## SUPPLEMENTAL INFORMATION

Supplemental information can be found online at https://doi.org/10.1016/j.isci.2024.111084.

Received: May 15, 2024
Revised: August 12, 2024
Accepted: September 27, 2024
Published: October 3, 2024

## REFERENCES

1. Demir, S., Nawroth, P.P., Herzig, S., and Ekim Üstünel, B. (2021). Emerging Targets in Type 2 Diabetes and Diabetic Complications. Adv. Sci. *8*, e2100275. https://doi.org/10.1002/advs.202100275.
2. Fisher, D.P., Johnson, E., Haneuse, S., Arterburn, D., Coleman, K.J., O'Connor, P.J., O'Brien, R., Bogart, A., Theis, M.K., Anau, J., et al. (2018). Association Between Bariatric Surgery and Macrovascular Disease Outcomes in Patients with Type 2 Diabetes and Severe Obesity. JAMA *320*, 1570–1582. https://doi.org/10.1001/jama.2018.14619.
3. Rocca, B., Rubboli, A., and Zaccardi, F. (2019). Antithrombotic therapy and revascularisation strategies in people with diabetes and coronary artery disease. Eur. J. Prev. Cardiol. *26*, 92–105. https://doi.org/10.1177/2047487319880045.
4. Reutens, A.T., and Atkins, R.C. (2011). Epidemiology of diabetic nephropathy. Contrib. Nephrol. *170*, 1–7. https://doi.org/10.1159/000324934.
5. Papatheodorou, K., Papanas, N., Banach, M., Papazoglou, D., and Edmonds, M. (2016). Complications of Diabetes 2016. J. Diabetes Res. *2016*, 6989453. https://doi.org/10.1155/2016/6989453.
6. Akhter, F., Salman Khan, M., Shahab, U., and Ahmad, S. (2013). Bio-physical characterization of ribose induced glycation: a mechanistic study on DNA perturbations. Int. J. Biol. Macromol. *58*, 206–210. https://doi.org/10.1016/j.ijbiomac.2013.03.036.
7. Anguizola, J.A., Basiaga, S.B.G., and Hage, D.S. (2013). Effects of Fatty Acids and Glycation on Drug Interactions with Human Serum Albumin. Curr. Metabolomics *1*, 239–250. https://doi.org/10.2174/2213235x1130100005.
8. Lee, J.E. (2015). Alternative biomarkers for assessing glycemic control in diabetes: fructosamine, glycated albumin, and 1,5-anhydroglucitol. Ann. Pediatr. Endocrinol. Metab. *20*, 74–78. https://doi.org/10.6065/apem.2015.20.2.74.
9. Qiu, H.Y., Hou, N.N., Shi, J.F., Liu, Y.P., Kan, C.X., Han, F., and Sun, X.D. (2021). Comprehensive overview of human serum albumin glycation in diabetes mellitus. World J. Diabetes *12*, 1057–1069. https://doi.org/10.4239/wjd.v12.i7.1057.
10. Wu, X.Q., Zhang, D.D., Wang, Y.N., Tan, Y.Q., Yu, X.Y., and Zhao, Y.Y. (2021). AGE/RAGE in diabetic kidney disease and ageing kidney. Free Radic. Biol. Med. *171*, 260–271. https://doi.org/10.1016/j.freeradbiomed.2021.05.025.
11. Chen, J., Huang, X., Halicka, D., Brodsky, S., Avram, A., Eskander, J., Bloomgarden, N.A., Darzynkiewicz, Z., and Goligorsky, M.S. (2006). Contribution of p16INK4a and p21CIP1 pathways to induction of premature senescence of human endothelial cells: permissive role of p53. Am. J. Physiol. Heart Circ. Physiol. *290*, H1575–H1586. https://doi.org/10.1152/ajpheart.00364.2005.
12. Sorci, G., Riuzzi, F., Giambanco, I., and Donato, R. (2013). RAGE in tissue

homeostasis, repair and regeneration. Biochim. Biophys. Acta *1833*, 101–109. https://doi.org/10.1016/j.bbamcr.2012.10.021.

13. Senatus, L.M., and Schmidt, A.M. (2017). The AGE-RAGE Axis: Implications for Age-Associated Arterial Diseases. Front. Genet. *8*, 187. https://doi.org/10.3389/fgene.2017.00187.
14. Schalkwijk, C.G., and Miyata, T. (2012). Early- and advanced non-enzymatic glycation in diabetic vascular complications: the search for therapeutics. Amino Acids *42*, 1193–1204. https://doi.org/10.1007/s00726-010-0779-9.
15. Prasad, K., and Mishra, M. (2017). Do Advanced Glycation End Products and Its Receptor Play a Role in Pathophysiology of Hypertension. Int. J. Angiol. *26*, 1–11. https://doi.org/10.1055/s-0037-1598183.
16. Sabbatinelli, J., Castiglione, S., Macrì, F., Giuliani, A., Ramini, D., Vinci, M.C., Tortato, E., Bonfigli, A.R., Olivieri, F., and Raucci, A. (2022). Circulating levels of AGEs and soluble RAGE isoforms are associated with all-cause mortality and development of cardiovascular complications in type 2 diabetes: a retrospective cohort study. Cardiovasc. Diabetol. *21*, 95. https://doi.org/10.1186/s12933-022-01535-3.
17. González, I., Morales, M.A., and Rojas, A. (2020). Polyphenols and AGEs/RAGE axis. Trends and challenges. Food Res. Int. *129*, 108843. https://doi.org/10.1016/j.foodres.2019.108843.
18. Wang, P., Chi, L., Zhang, Z., Zhao, H., Zhang, F., and Linhardt, R.J. (2022). Heparin: An old drug for new clinical applications. Carbohydr. Polym. *295*, 119818. https://doi.org/10.1016/j.carbpol.2022.119818.
19. Schwartz, B.S. (1990). Heparin: what is it? How does it work. Clin. Cardiol. *13*. VI12–15.
20. Beurskens, D.M.H., Huckriede, J.P., Schrijver, R., Hemker, H.C., Reutelingsperger, C.P., and Nicolaes, G.A.F. (2020). The Anticoagulant and Nonanticoagulant Properties of Heparin. Thromb. Haemostasis *120*, 1371–1383. https://doi.org/10.1055/s-0040-1715460.
21. Chiodelli, P., Bugatti, A., Urbinati, C., and Rusnati, M. (2015). Heparin/Heparan sulfate proteoglycans glycomic interactome in angiogenesis: biological implications and therapeutical use. Molecules *20*, 6342–6388. https://doi.org/10.3390/molecules20046342.
22. Berdiaki, A., Neagu, M., Giatagana, E.M., Kuskov, A., Tsatsakis, A.M., Tzanakakis, G.N., and Nikitovic, D. (2021). Glycosaminoglycans: Carriers and Targets for Tailored Anti-Cancer Therapy. Biomolecules *11*, 395. https://doi.org/10.3390/biom11030395.
23. Yu, L.J., Ko, V.H., Tsikis, S.T., Dao, D.T., Secor, J.D., Pan, A., Cho, B.S., Michell, P.D., Fligor, S.C., Kishikawa, H., and Puder, M. (2023). Effects of systemic anticoagulation in a murine model of compensatory lung growth. Pediatr. Res. *93*, 1846–1855. https://doi.org/10.1038/s41390-022-02323-1.
24. Rao, N.V., Argyle, B., Xu, X., Reynolds, P.R., Walenga, J.M., Prechel, M., Prestwich, G.D., MacArthur, R.B., Walters, B.B., Hoidal, J.R., and Kennedy, T.P. (2010). Low anticoagulant heparin targets multiple sites of inflammation, suppresses heparin-induced thrombocytopenia, and inhibits interaction of RAGE with its ligands. Am. J. Physiol. Cell Physiol. *299*, C97–C110. https://doi.org/10.1152/ajpcell.00009.2010.
25. Patil, B., Meena, L.N., Sharma, D.C., Agarwal, G., Dadhich, Y., and Gupta, G. (2022). Impact of low-molecular-weight heparin in the treatment of moderately severe and severe acute pancreatitis; a randomized, single blind, phase 3 control trial. Int. J. Surg. *101*, 106621. https://doi.org/10.1016/j.ijsu.2022.106621.
26. Pan, Q., Zhang, C., Wu, X., and Chen, Y. (2020). Identification of a heparosan heptasaccharide as an effective anti-inflammatory agent by partial desulfation of low molecular weight heparin. Carbohydr. Polym. *227*, 115312. https://doi.org/10.1016/j.carbpol.2019.115312.
27. Mu, S., Liu, Y., Jiang, J., Ding, R., Li, X., Li, X., and Ma, X. (2018). Unfractionated heparin ameliorates pulmonary microvascular endothelial barrier dysfunction via microtubule stabilization in acute lung injury. Respir. Res. *19*, 220. https://doi.org/10.1186/s12931-018-0925-6.
28. Sick, E., Brehin, S., André, P., Coupin, G., Landry, Y., Takeda, K., and Gies, J.P. (2010). Advanced glycation end products (AGEs) activate mast cells. Br. J. Pharmacol. *161*, 442–455. https://doi.org/10.1111/j.1476-5381.2010.00905.x.
29. Mizumoto, S., Takahashi, J., and Sugahara, K. (2012). Receptor for advanced glycation end products (RAGE) functions as receptor for specific sulfated glycosaminoglycans, and anti-RAGE antibody or sulfated glycosaminoglycans delivered in vivo inhibit pulmonary metastasis of tumor cells. J. Biol. Chem. *287*, 18985–18994. https://doi.org/10.1074/jbc.M111.313437.
30. Xu, D., and Esko, J.D. (2014). Demystifying heparan sulfate-protein interactions. Annu. Rev. Biochem. *83*, 129–157. https://doi.org/10.1146/annurev-biochem-060713-035314.
31. Bishop, J.R., Schuksz, M., and Esko, J.D. (2007). Heparan sulphate proteoglycans fine-tune mammalian physiology. Nature *446*, 1030–1037. https://doi.org/10.1038/nature05817.
32. Frolova, N., Soboleva, A., Nguyen, V.D., Kim, A., Ihling, C., Eisenschmidt-Bönn, D., Mamontova, T., Herfurth, U.M., Wessjohann, L.A., Sinz, A., et al. (2021). Probing glycation potential of dietary sugars in human blood by an integrated in vitro approach. Food Chem. *347*, 128951. https://doi.org/10.1016/j.foodchem.2020.128951.
33. Jin, Y.J., Chennupati, R., Li, R., Liang, G., Wang, S., Iring, A., Graumann, J., Wettschureck, N., and Offermanns, S. (2021). Protein kinase N2 mediates flow-induced endothelial NOS activation and vascular tone regulation. J. Clin. Invest. *131*, e145734. https://doi.org/10.1172/JCI145734.
34. Kim, T.K., Jeon, S., Park, S., Sonn, S.K., Seo, S., Suh, J., Jin, J., Kweon, H.Y., Kim, S., Moon, S.H., et al. (2022). 2′-5′ oligoadenylate synthetase-like 1 (OASL1) protects against atherosclerosis by maintaining endothelial nitric oxide synthase mRNA stability. Nat. Commun. *13*, 6647. https://doi.org/10.1038/s41467-022-34433-z.
35. Shen, W., Song, Z., Zhong, X., Huang, M., Shen, D., Gao, P., Qian, X., Wang, M., He, X., Wang, T., et al. (2022). Sangerbox: A comprehensive, interaction-friendly clinical bioinformatics analysis platform. iMeta *1*, e36. https://doi.org/10.1002/imt2.36.
36. Su, L., Hershberger, R.J., and Weissman, I.L. (1993). LYAR, a novel nucleolar protein with zinc finger DNA-binding motifs, is involved in cell growth regulation. Genes Dev. *7*, 735–748. https://doi.org/10.1101/gad.7.5.735.
37. Miyazawa, N., Yoshikawa, H., Magae, S., Ishikawa, H., Izumikawa, K., Terukina, G., Suzuki, A., Nakamura-Fujiyama, S., Miura, Y., Hayano, T., et al. (2014). Human cell growth regulator Ly-1 antibody reactive homologue accelerates processing of preribosomal RNA. Gene Cell. *19*, 273–286. https://doi.org/10.1111/gtc.12129.
38. Kojimahara, M. (1988). Intimal laminated elastosis in the intrarenal arteries. An electron microscopic study. Acta Pathol. Jpn. *38*, 315–323. https://doi.org/10.1111/j.1440-1827.1988.tb02304.x.
39. Di Marco, E., Gray, S.P., Kennedy, K., Szyndralewiez, C., Lyle, A.N., Lassègue, B., Griendling, K.K., Cooper, M.E., Schmidt, H.H.H.W., and Jandeleit-Dahm, K.A.M. (2016). NOX4-derived reactive oxygen species limit fibrosis and inhibit proliferation of vascular smooth muscle cells in diabetic atherosclerosis. Free Radic. Biol. Med. *97*, 556–567. https://doi.org/10.1016/j.freeradbiomed.2016.07.013.
40. Tuleta, I., and Frangogiannis, N.G. (2021). Diabetic fibrosis. Biochim. Biophys. Acta, Mol. Basis Dis. *1867*, 166044. https://doi.org/10.1016/j.bbadis.2020.166044.
41. Yang, C., Liu, X., Cheng, T., Xiao, R., Gao, Q., Ming, F., Jin, M., Chen, H., and Zhou, H. (2019). LYAR Suppresses Beta Interferon Induction by Targeting Phosphorylated Interferon Regulatory Factor 3. J. Virol. *93*, e00769-19. https://doi.org/10.1128/JVI.00769-19.
42. Al-Kuraishy, H.M., Al-Gareeb, A.I., Alkazmi, L., Habotta, O.A., and Batiha, G.E.S. (2022). High-mobility group box 1 (HMGB1) in COVID-19: extrapolation of dangerous liaisons. Inflammopharmacology *30*, 811–820. https://doi.org/10.1007/s10787-022-00988-y.
43. Jantscheff, P., Schlesinger, M., Fritzsche, J., Taylor, L.A., Graeser, R., Kirfel, G., Fürst, D.O., Massing, U., and Bendas, G. (2011). Lysophosphatidylcholine pretreatment reduces VLA-4 and P-Selectin-mediated b16.f10 melanoma cell adhesion in vitro and inhibits metastasis-like lung invasion in vivo. Mol. Cancer Therapeut. *10*, 186–197. https://doi.org/10.1158/1535-7163.MCT-10-0474.
44. Nair, A., Morsy, M.A., and Jacob, S. (2018). Dose translation between laboratory animals and human in preclinical and clinical phases of drug development. Drug Dev. Res. *79*, 373–382. https://doi.org/10.1002/ddr.21461.

## STAR★METHODS

### KEY RESOURCES TABLE

| REAGENT or RESOURCE | SOURCE | IDENTIFIER |
|---|---|---|
| Antibodies | | |
| RAGE antibody | Abcam | ab216329; RRID:AB_2884897 |
| Donkey anti-rabbit IgG H&L (Alexa Fluor® 488) | Abcam | ab150073; RRID: AB_2636877 |
| NF-κB antibody | CST | 8242; RRID: AB_10859369 |
| LYAR antibody | Abcam | ab233082; RRID: AB_3662637 |
| GAPDH antibody | Proteintech | 10494-1-AP; RRID: AB_2263076 |
| Goat anti-rabbit IgG (H + L) | Beyotime | A0208; RRID: AB_2892644 |
| CD31 | ServiceBio | GB11063-2; RRID: AB_2922436 |
| Chemicals, peptides, and recombinant proteins | | |
| Human serum albumin (HSA) | Sigma | A3782 |
| PBS | Solarbio | P1020 |
| Glucose | Sigma | 158968 |
| Sodium azide | Sigma | S8032 |
| Heparin | BBI Life Sciences | Biochemical grade, 6–20 kD |
| BCA kit | Solarbio | PC0020 |
| Enhanced CCK8 kit | Spark Jade | CT0001-A |
| Annexin V-FITC/PI apoptosis kit | Multi Sciences | AP101-100-Kit |
| NO concentration assay kit | Beyotime | S0021s |
| eNOS activity assay kit | Beyotime | S0025 |
| RPMI 1640 | Gibco | 11875093 |
| FBS | ExCell Bio | FSP500 |
| EDTA trypsin digestion solution | Solarbio | T1300 |
| Penicillin-streptomycin mixture | Solarbio | P1400 |
| FITC-BSA | Solarbio | SF063 |
| 4% paraformaldehyde solution | Biosharp | BL539A |
| Triton X-100 | Solarbio | T8200 |
| Bovine serum albumin | Solarbio | A8020 |
| DAPI | Solarbio | C0065 |
| SDC (Sodium deoxycholate) | Sigma | D6750-10G |
| Urea | Sigma | U5128-100G |
| ECL chemiluminescence kit | EASEN | 36208Y |
| TRIzol reagent | Ambion | 340312 |
| PrimeScript™ RT reagent Kit with gDNA Eraser | TaKaRa | RR047A |
| TB Green® Premix Ex Taq™ II | TaKaRa | RR820A |
| DTT (Dithiothreitol) | Sigma | D9779 |
| IAA (Iodoacetamide) | Sigma | I1149 |
| TCA (Trichloroacetic acid) | Sigma | T0699 |
| Trypsin Gold, Mass Spectrometry Grade | Promega | V5280 |
| Streptozotocin | Sigma | V900890 |
| Acetonitrile (Mass spectrometry grade) | Thermo Scientific | A955-4 |
| Formic acid (Mass spectrometry grade) | Thermo Scientific | A1170-50 |
| $H_2O$ (Mass spectrometry grade) | Thermo Scientific | W6-4 |

(*Continued on next page*)

*Continued*

| REAGENT or RESOURCE | SOURCE | IDENTIFIER |
|---|---|---|
| Oligonucleotides | | |
| RAGE primer:<br>For: 5′-AGTGTGGCTCGTGTCCTTCC-3′,<br>Rev: 5′TCTCCTTTCCATTCCTGTTCATTGC-3′ | OBIO | N/A |
| GAPDH primer:<br>For: 5′-ACCCACTCCTCCACCTTTGAC-3′,<br>REV: 5′-TCCACCACCCTGTTGCTGTAG-3′. | OBIO | N/A |
| siRNA LYAR:<br>For: GGAUGAAGAACAGUUUAAATT;<br>Rev: UUUAAACUGUUCUUCAUCCTT. | OBIO | N/A |
| Deposited data | | |
| Raw and analyzed data | This paper | IProX: IPX0009808000 |
| Experimental models: Organisms/strains | | |
| Mouse: C57BL/6J | Pengyue Co., Ltd. | SCXK20190003 |
| Experimental models: Cell lines | | |
| HUVECs | ATCC | CRL-1730 |
| Software and algorithms | | |
| Prism 9.0 | GraphPad Software | N/A |
| Proteome Discoverer | Thermo Scientific | Version 1.4 |
| Sanger box platform | Hangzhou Mugu Technology Co., Ltd | http://sangerbox.com/ |
| Cytoscape | | https://cytoscape.org/ |

## EXPERIMENTAL MODEL AND STUDY PARTICIPANT DETAILS

### Cells

HUVECs (ATCC, passage number, p+10) were cultured in roswell park memorial institute (RPMI) medium 1640 (Gibco) supplemented with 10% fetal bovine serum (FBS) (ExCell Bio) and 1% penicillin-streptomycin mixture (Solarbio). Cells were professionally certified and tested for mycoplasma contamination.

### Mice

Male C57BL/6J mice (Pengyue Laboratory, Jinan, China) were used to establish the diabetic mouse model. Streptozotocin (Sigma) 50 mg/kg was injected for five consecutive days. One week later, blood glucose $\geq$11.1 mmol/L was used as the standard to determine whether the model was established. All the procedures performed in this study were approved by the Animal Ethics Committee of Shandong Second Medical University (2022SDL095). All procedures were performed with relevant guidelines and laws.

## METHOD DETAILS

### AGEs preparation and analysis

To prepare AGEs, 1 g of human serum albumin (HSA, Sigma) was dissolved in PBS containing 0.5 M glucose (Sigma) and 0.05% sodium azide, resulting in a final concentration of 50 mg/mL. Then, the mixture was incubated at 37°C for 90 days to enable glycation. After the reaction, fluorescence characteristics of HSA were detected using a fluorescence chromatography system with an excitation wavelength $\lambda$ex = 355 nm and an emission wavelength $\lambda$em = 460 nm over a period of 0–13 weeks.

Protein desalting was performed by 30 kDa centrifugal filters. The protein concentration was determined with BCA kit (PC0020, Solarbio). Next, 10 mg aliquots were lyophilized and then reconstituted in water at the final concentration of 1 μg/μL. The proteins were separated using an HPLC $C_{18}$ pre-column (1 mm × 8 mm, 5.0 μL) and subjected to direct analysis by Q Exactive Plus mass spectrometer (Thermo Scientific). MS data were processed using MagTran software to calculate the molecular weights of the proteins.

### Measurement of cell viability in response to AGEs stimulation

Cells were detached using a EDTA trypsin digestion solution (Solarbio) at the density of 80%–90%. The AGEs at the concentration of 0, 50, 200, 400 and 800 μg/mL were prepared in RPMI medium 1640 with 2.5% FBS and 1% penicillin-streptomycin mixture. Subsequently, 5000 cells per

well were inoculated in 96-well plates and cultured in a $CO_2$ incubator (Thermo Scientific) for 24 h. 10 μL of CCK8 (Spark Jade) was then added to each well for an additional 2 h. Cell viability was determined by measuring the optical density value at 450 nm using a Multiskan FC enzyme standard instrument (Thermo Scientific).

### Cell biological and biochemical assays

HUVECs were divided into CT group, 800 μg/mL AGEs group and 200 μg/mL heparin (BBI Life Sciences Corporation, Biochemical grade, 6–20 kD) + 800 μg/mL AGEs group. NO concentration and eNOS activity were measured with corresponding assay kits (Beyotime). Cells were cultured in 10 cm dishes (Servicebio) for 24 h, and subsequently digested with EDTA trypsin. The number of cells was counted by countstar instrument. Annexin V-FITC/PI apoptosis kit (Multi Sciences) and DxFLEX flow cytometry (Beckman Coulter) were utilized for apoptosis detection.

For endothelial cell permeability, $2\times10^5$ cells were seeded into 12-well plate and treated for 24 h under the corresponding conditions. Then the 100 μg/mL FITC-BSA was incubated with cells for 1h and detected by laser confocal scanning microscopy.

### Immunofluorescence

To visualize the expression pattern of RAGE, cells were cultured on slides and subjected to AGEs and heparin stimulation for 24 h. The slides were prepared by cleaning with 75% ethanol and PBS, followed by incubation with 80,000 cells. After stimulation, cells were fixed with a 4% paraformaldehyde solution (Biosharp) for 10 min. Subsequently, cells were permeabilized with 0.025% Triton X-100 (Solarbio) for 5 min and blocked with 5% bovine serum albumin (Solarbio) for an additional 30 min. Next, cells were incubated overnight with RAGE antibody (1:500; Abcam Cat# ab216329, RRID: AB_2884897) and subsequently with donkey anti-rabbit IgG H&L (Alexa Fluor 488) (1:500; Abcam Cat# ab150073, RRID: AB_2636877) for 1 h at room temperature. Expression patterns of RAGE were captured using a scanning electron microscope (Zeiss) after DAPI (4,6-Diamidino-2-phenylindole) incubation for 10 min.

### Western blotting

Cells were lysed with SDC (Sodium deoxycholate, Sigma) urea lysis buffer for 10 min and centrifuged at 12000 rpm at 4°C for 10 min. The BCA kit was used to measure the protein concentration in supernatant. Proteins were loaded and separated by electrophoresis on 10%–12% sodium dodecyl sulphate-polyacrylamide gel (SDS-PAGE). Then, they were transferred to the polyvinylidene fluoride (PVDF) membrane, block with 5% skimmed milk powder for 1 h. Primary antibodies RAGE (Abcam Cat# ab216329, RRID: AB_2884897), NF-κB (#8242, CST), LYAR (Cell growth-regulating nucleolar protein, ab233082, Abcam) and GAPDH (Proteintech Cat# 10494-1-AP, RRID: AB_2263076) were incubated overnight at 4°C. They were also incubated with horseradish peroxidase conjugated goat anti-rabbit IgG (H + L) (Beyotime Cat# A0208, RRID: AB_2892644) for 1.5 h. Finally, the ECL chemiluminescence kit (36208Y, EASEN) was used for exposure.

### Reverse transcription polymerase chain reaction analysis

Total RNA was extracted from the cells using TRIzol reagent (Ambion) and reverse transcribed with the PrimeScript RT reagent Kit with gDNA Eraser (RR047A, TaKaRa). Amplification was performed using TB Green Premix Ex Taq II (RR820A, TaKaRa), and quantitative polymerase chain reaction (qPCR) analysis was conducted. Cycle threshold (Ct) and $2^{-\Delta\Delta Ct}$ were calculated to determine gene expression levels. The *RAGE* forward primer was 5′-AGTGTGGCTCGTGTCCTTCC-3′, and the reverse primer was 5′-TCTCCTTTCCATTCCTGTTCATTGC-3′. For *GAPDH*, the forward primer was 5′-ACCCACTCCTCCACCTTTGAC-3′, and the reverse primer was 5′-TCCACCACCCTGTTGCTGTAG-3′. Relative *RAGE* gene expression levels were normalized to *GAPDH* expression.

### LC-MS/MS analysis

Cells were lysed by SDC-urea buffer and sonicated at 250 W for 1 min (3 s on, 7 s off). Protein concentration was determined after centrifugation. 100 μg proteins were reduced by 20 mM DTT (Dithiothreitol, Sigma) at 56°C for 30 min, and alkylated with a 40 mM IAA (Iodoacetamide, Sigma) solution at room temperature in the dark for 30 min. The proteins were precipitated by 10% TCA (Trichloroacetic acid, Sigma) and incubated at −20°C for 2 h. Samples were thawed, centrifuged, and the supernatant was discarded. Cold acetone (0.5 mL) was added, followed by another centrifugation and drying using a vacuum concentrator (Jiaimu). Proteins were digested with Trypsin Gold (Mass Spectrometry Grade, Promega 1:25, w/w) and incubated at 37°C overnight.

nanoLC-MS/MS analysis was performed on the Orbitrap Eclipse Tribrid mass spectrometer (Thermo Scientific). Solvent A was 0.1% formic acid (FA) in water, and Solvent B was 0.1% FA in 80% acetonitrile (ACN). Peptides were re-dissolved and loaded onto the $C_{18}$ trap column (Thermo Scientific Acclaim PepMap, 75 μm × 20 mm, 3 μm, 100 Å) and separated by the $C_{18}$ analytical column (Thermo Scientific Acclaim PepMap RSLC, 75 μm × 25 cm, 2 μm, 100 Å). The gradient was set as follows: 0–54 min, 5%–35% B; 54–59 min, 35%–50% B; 59–67 min, 50%–95% B; 67–75 min, 95% B with a flow rate of 300 nL/min. Mass spectrometry operated in the positive ion mode with specific parameters.

### Cell transfection experiments

Small interfering RNA (siRNA) oligonucleotides and untargeted interfering control siRNA for human LYAR (For: GGAUGAA GAACAGUUUAAATT; Rev: UUUAAACUGUUCUUCAUCCTT) were purchased from OBIO (Shanghai, China). HUVECs were seeded in 10 cm dish and transfected with 100 nM siRNA-LYAR using Lipofectamine 3000 (Invitrogen) in Opti-MEM (Thermo Scientific), as described

in the manufacturer's protocol (siRNA negative control was added to other groups). After 24 h, the fresh cell culture medium was replaced and cultured for another 24 h under different simulations.

### Animals experimental

Eight-week-old male C57BL/6J mice were adaptive feeding with normal diet for one week, the mice were randomly divided into control (CT) group, DM group and heparin group, with 10 mice in each group. Streptozotocin (Sigma) 50 mg/kg was injected for five consecutive days in DM and heparin groups. One week later, blood glucose $\geq$ 11.1 mmol/L was used as the standard to determine whether the model was established. In consideration of the weight of diabetic mice (23.2 $\pm$ 1.8 g), 50 IU heparin (dissolved in saline) was injected subcutaneously daily in heparin group,[43] and those in the DM and CT groups were injected with normal saline as control. The dosage of heparin was approximately 12 times higher than the human equivalent dose per unit body weight.[44] After 35 days of continuous injection, mice were anesthetized with sodium pentobarbital and the mid-thoracic aorta was harvested.

### Histopathological and immunohistochemical analysis

Vascular specimens were immediately fixed in 4% paraformaldehyde after sampling, embedded in paraffin, and sectioned at 5 μm thickness. Histopathological analysis was performed using hematoxylin-eosin (H&E), masson and sirius red staining. In immunohistochemical (IHC) analysis, CD31 (ServiceBio Cat# GB11063-2, RRID: AB_2922436), LYAR and NF-κB were used as primary antibodies, respectively, combined with homologous secondary antibodies. The cells were stained with 3,3′-diaminobenzidine (DAB) and the nuclei were counterstained with hematoxylin. Photographs were obtained using motic digital pathology solution (Motic).

## QUANTIFICATION AND STATISTICAL ANALYSIS

At least 3 experimental data were used for statistical evaluation in each group. Data were analyzed using GraphPad Prism, ordinary one-way ANOVA (multiple comparisons) was used for group comparisons. $p < 0.05$ was considered to indicate statistical significance. Proteome Discoverer software (Thermo Fisher Scientific, Version 1.4) was used for peptide search and ratio calculation from raw data. Significantly changed peptides had a fold change cutoff of 1.3, adjusted *q-value* < 0.05, and *FDR* < 0.01. Bioinformatics analyses, including volcano plots, Venn diagrams, and gene ontology (GO) and Kyoto encyclopedia of genes and genomes (KEGG) function enrichment of differential proteins, were conducted using the Sanger box platform. Protein interaction networks were analyzed using the String website, and proteins with a high confidence score (0.7) were selected for functional interpretation through Cytoscape visualization.